

PROCESSING OF DRONE-BORNE HYPERSPECTRAL DATA FOR GEOLOGICAL APPLICATIONS

Sandra Jakob, Robert Zimmermann, Richard Gloaguen

Helmholtz-Zentrum Dresden-Rossendorf

Helmholtz Institute Freiberg for Resource Technology, Division of Exploration, Chemnitzer Straße 40,
09599 Freiberg

ABSTRACT

Unmanned Aerial Systems (UAS) are used increasingly to close the gap between space- or airborne and field spectral data. They are able to provide high-resolution hyperspectral images within a short time. However, complex geometric and radiometric corrections are required. These correction steps are crucial, especially when the data should be used in geological applications such as detection of raw materials. Thus, in the following paper we present a new toolbox for processing drone-borne hyperspectral data. Processing steps comprise automatic co-registration, mosaicking and georeferencing as well as topographic and illumination correction. For the first time we show the applicability of drone-borne hyperspectral data for geological surveys.

Index Terms— hyperspectral data, Unmanned Aerial Systems, drone-borne remote sensing, processing toolbox, Acidic Mine Drainage

1. INTRODUCTION

Hyperspectral mapping has become a common tool for various applications in remote sensing. Space- and airborne hyperspectral data cover large areas and are widely used in geology, mineral mapping and exploration [1, 2]. However, compared to field spectrometric data, they often suffer from spectral and spatial resolution and low signal-to-noise ratios, caused by the difficult and complex atmospheric correction. Additionally, the surveys for data acquisitions are time- and cost-consuming and need extensive planning. In the last years, more and more lightweight hyperspectral sensors have been developed for use on unmanned aerial systems [3, 4]. These sensors are able to close the gap between field- and air- or spaceborne data and provide small-scale high-resolution hyperspectral surveys with a heavily decreased influence of the atmosphere. Nevertheless, geometric correction of drone-borne data is challenging. However, due to limitations in weight and power consumption of the sensor only the visible and near-infrared (VNIR) part of the electromagnetic spectrum can be covered. Hence, until now, these systems have been mainly used for vegetation mapping, precision agriculture and

environmental studies [5, 6], but not for geological applications such as mineral mapping. In the following, we present a data processing chain that enables an accurate geometric and radiometric correction of drone-borne hyperspectral images. Additionally, the applicability for geological surveys is evaluated. All correction steps are implemented in a Python toolbox.

2. STUDY AREA

The two presented test sites are located in the Eger Graben of the Czech Republic near the city of Sokolov (Fig. 1). The Eger Graben is filled with tertiary sediments with thick layers of lignite. The abandoned lignite mine of Sylvester provides a high relief. It is thus excellent to test several topographic correction approaches. The Litov dump has been analyzed and mapped earlier by Kopackova et al. [7] for acid mining drainage using airborne hyperspectral data.

3. SETUP AND DATA ACQUISITION

3.1. Aerial platform

Two commercially available UAS were used for data acquisition. One is the Aibotix Aibot X6v2 hexacopter with a maximum payload of up to 2 kg and a flight time of about 15 min [8]. With a take-off weight of about 5 kg it can be used to rapidly and easily cover small-scale definite areas. The Aibot can carry various sensors, such as RGB and hyperspectral cameras or geophysical instruments. The 3D-gyroscope ensures nadir orientation of the sensor at any time. The Aibot were flown with a RIKOLA hyperspectral camera and a NIKON Coolpix A for photogrammetry. The senseFly eBee [9] is a fully autonomous fixed-wing drone with a take-off weight of 0.69 kg and 50 min flight time. It allows for acquisition of detailed high-resolution images of an area of up to 10 km². Using Structure-from-Motion photogrammetric software, orthophotos (Fig. 1) and digital surface models can be computed, which will be needed for the georeferencing and topographic correction of the hyperspectral images. The senseFly eBee is equipped with a Canon S110 RGB digital camera.

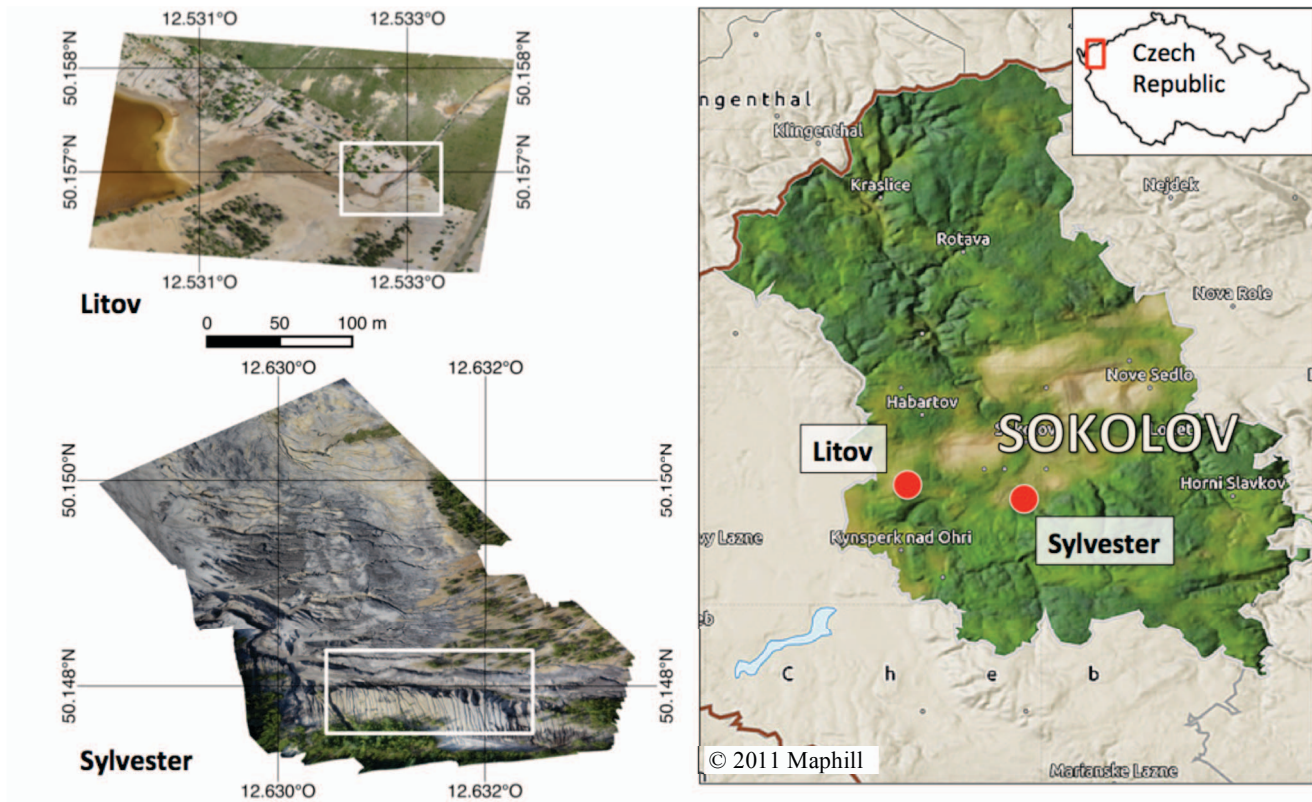


Fig. 1: Test site orthophotos (left) and locations (right). The white rectangles mark the flightsites for hyperspectral images.

3.2. Hyperspectral sensor

A frame-based hyperspectral camera of Rikola Ltd. [3] was used for data acquisition. With its low weight of about 720 gram it is perfectly suitable for drone-borne surveys. The sensor provides snapshot images covering the VIS-NIR spectral range between 504 and 900 nm. In the autonomous mode, up to 50 bands with a spectral resolution of >10 nm and spectral steps of 1 nm can be acquired within one flight. The maximum image dimensions account for 1024 x 1011 true image pixels. For flight images the spatial resolution is half the size to enable the maximum number of spectral bands.

3.3. Flightsite setup

The UAS-survey commonly comprises several flights. The sensefly eBee is used to rapidly cover a large area with RGB-images for the generation of the orthophoto and DSM. Parts of the study area with complex topography or steep slopes can be additionally surveyed using the Aibot with an RGB-camera. In this way, accuracy and resolution of orthophoto and DSM can be increased distinctly. Processing of both is done using the commercial photogrammetry software *Agisoft Photoscan*.

The hyperspectral survey is commonly done with multiple flights, depending on the size of the area and the required spectral ranges. Within the surveyed area calibration panels

are placed. We use a black, a grey and a white PVC panel. Their spectra were determined using a Spectral Evolution PSR-3500 portable field spectrometer and are relatively consistent in the VNIR spectral range. Additional GCP points can be placed within the study area for later validation of the automatic geo-referencing. The number and distribution of the spectral band is set before the flight and uploaded as taskfile on a CF memory card, which will store the acquired images. The integration time of the hyperspectral sensor is set according to the illumination conditions and accounts for about 10 ms for sunny weather and 40-50 ms for completely cloudy days.

4. CORRECTION STEPS

4.1. Dark current subtraction and conversion to radiance

A dark calibration is needed to determine the Dark Current (DC) of the camera's sensor. For this, the camera is triggered under completely light-free conditions by entirely covering the camera lens. The resulting data can be later subtracted from the acquired raw image Digital Numbers (DN). The DC-subtraction itself is done with the *Hyperspectral Imager* software provided by Rikola Ltd. This software is also used to calibrate the image data for vignetting as well as some camera specific values and convert the raw DN to radiance.

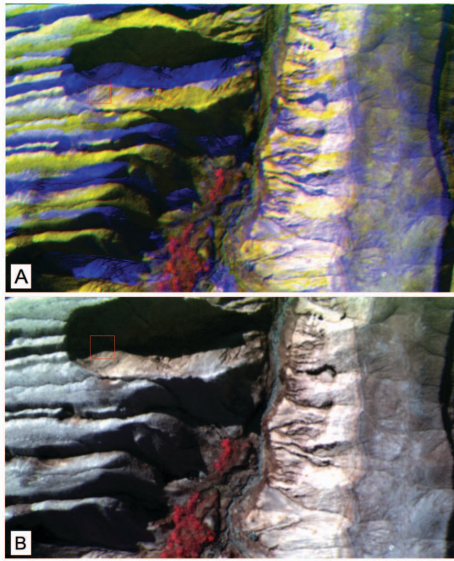


Fig. 2: Rikola false color image, before (A) and after (B) co-registration

4.2. Internal camera distortions

Distortions caused by internal camera features lead mainly to radial and tangential distortions, e.g. Berni et al. [10]. Radial distortions are caused by the shape of the lens and mostly become visible as "barrel" or "fish-eye" effect. Tangential distortions can be caused by a non-parallel assembly of the lens with respect to the image plane. The lens distortion parameters of the RIKOLA hyperspectral camera were determined using *Agisoft Lens*, which uses a checkerboard pattern that is either projected on a flat screen or printed out. At least ten images need to be acquired from different view angles and orientations. Using these images, internal camera parameters as well as the distortion coefficients can be calculated. The internal parameters can be expressed by the characteristic camera matrix, which includes focal length (f_x and f_y), skew, and center coordinates (c_x and c_y). The distortion coefficient matrix comprises the radial distortion coefficients k_1 , k_2 , k_3 , and the tangential distortion coefficients p_1 and p_2 . The determined parameters are used to correct the lens distortion.

4.3. Co-registration

The acquisition of the single spectral bands happens with a small temporal difference. Dependent on speed, movement and vibrations of the aerial platform, this results in a small spatial shift between the single bands of the hyperspectral data cube [11], see also Fig. 2, A. The correction of this mismatch is done using an automatic image-matching algorithm [12]. First characteristic features within the

several bands are detected, and then matching pairs of the detected points are identified. An affine transformation matrix is calculated from the calculated point pairs, which considers translation, rotation, shift and shear and corrects the mismatch with high precision (Fig. 2, B).

4.4. Mosaicking and illumination correction

Overlapping images of a survey were automatically mosaicked using an image-matching algorithm. This time, additional perspective distortions were considered. Optional an illumination correction between the several images can be applied. It uses overlapping points of the images to calculate a regression function. This function is afterwards applied to correct brightness differences caused by slightly changing illumination conditions during the acquisition of different images.

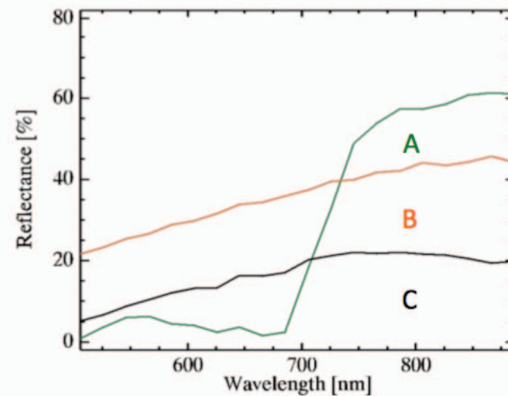
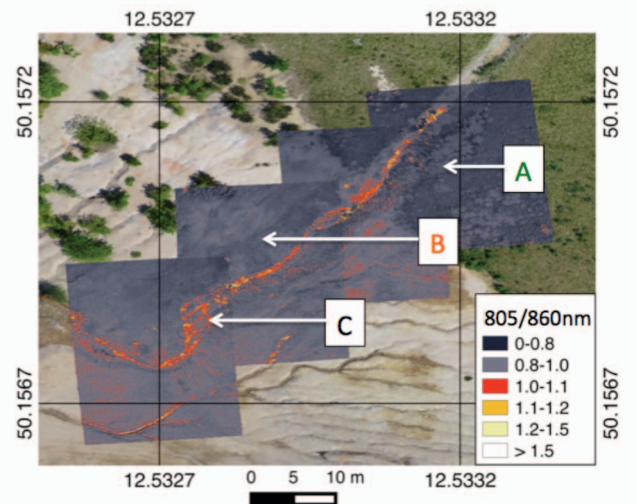


Fig. 3: Ratio of the 805 and 860 nm band of the geometrically and radiometrically corrected mosaic of a drainage system at Litov site and example reflectance spectra.

4.5. Automatic geo-referencing

The orthomosaic generation using Agisoft Photoscan includes a high-precision geo-referencing. Therefore, a high-resolution orthophoto is computed as base image for an automatic geo-referencing of the hyperspectral mosaic. The automatic geo-referencing uses an image-matching algorithm to fit the hyperspectral mosaic to the RGB orthophoto. The use of a non-adaptive transformation matrix can provide good results, but can also lead to misfits or inaccuracies, if illumination differences or topography-based distortions between orthophoto and hyperspectral mosaic are too high. Therefore, an adaptive transformation method is used to improve the fitting.

4.6. Topographic correction

Topography can have high influence on the local illumination within an image. Hence, same material can appear differently if it is located on a slope oriented towards or away from the sun light incidence. It is essential to correct for these effects to get reliable data. We implemented and tested the most common topographic correction methods to aim for an optimal correction result. The methods comprise several Lambertian as well as non-Lambertian methods, as mentioned in Richter et al. [13]. A digital surface model (DSM) having at least a similar spatial resolution is required for all methods. Furthermore, the sun elevation angle and sun azimuth present at the acquisition time is needed.

4.7. Conversion to reflectance

Subsequent to geometric and illumination corrections, the hyperspectral radiance image can be converted to reflectance. The influence of the atmosphere is nearly negligible due to the low acquisition height. Thus, no atmospheric correction is applied. The empirical line method is recommended instead [14]. It is a more direct approach using spectrally well-characterized ground reference targets. Thereby, the image spectra of the panels are extracted and compared to reference spectra. Correction factors are estimated for each band and applied using a linear regression function.

5. DISCUSSION AND CONCLUSION

An example for a completely geometrically and radiometrically corrected hyperspectral mosaic is shown in Fig. 3. It comprises a main drainage system at Litov site. For topographic correction a non-Lambertian method achieved the best results. Green vegetation can be easily distinguished from soil by the characteristic spectrum including the red

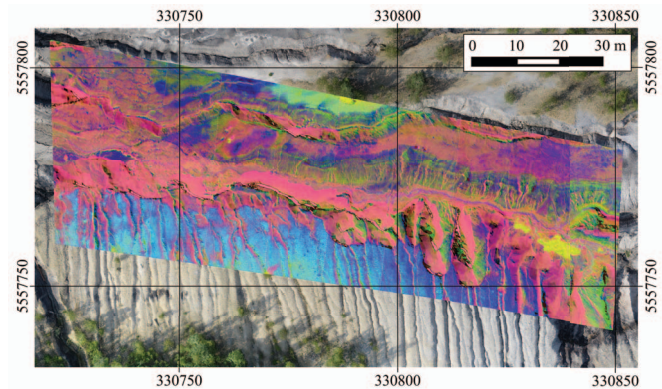


Fig. 4: MNF (1,2,3) of hyperspectral mosaic at Sylvester site

edge at 700 nm (Fig. 3, A). However, also several types of sediment can be differentiated, e.g., Fig. 3, B and C. Their detection is mainly based on differences in type and content of iron minerals, causing a varying slope of reflectance at the end of the spectrum between 800 and 900 nm (Fe^{3+} absorption). This could be the basis for general statements on trends of distribution of pH-characteristic minerals [7]. In our example, a general trend to the enhanced occurrence of iron minerals within the dump wastewater drainage system (Fig. 3, B) compared to outer sediments (Fig. 3, C) can be drawn.

Sylvester site shows higher incision in topography compared to Litov. Additionally, the images were captured in the late evening to simulate extreme illumination conditions. Not all topographic correction methods were applicable in this case. Some methods generally delivering good results cannot be used for completely shadowed areas, which often occur in steep terrain. However, geometric and radiometric image correction achieved good results. The application of Minimum Noise Fraction (MNF) enhances nearly no illumination differences between the individual images of the mosaic (Fig. 4).

The described workflow shows the applicability of our correction toolbox for hyperspectral drone-borne images and the usability of the created data for geological and environmental applications. We are able to correct for platform-caused shifts and distortions between individual bands. Geometric and radiometric corrections provide good results even in bad illumination conditions and steep terrain. Topographic correction eliminates relief-caused illumination differences, which could otherwise lead to the false detection of different materials in homogenous areas. We showed, that the corrected hyperspectral mosaics can be used for geological applications, such as detecting trends in mineralogy and soil composition. In combination with the fast and spontaneous acquisition using UAS, it is possible to provide high quality hyperspectral data for geological surveys rapidly and with high spatial and spectral resolution.

11. REFERENCES

- [1] F. D. van der Meer, H.M. van der Werff, F.J. van Ruitenbeek, C.A. Hecker, W.H. Bakker, M.F. Noomen, M. van der Meijde, E.J.M. Carranza, J.B. de Smeth, and T. Woldai, "Multi- and hyperspectral geologic remote sensing: A review", *International Journal of Applied Earth Observation and Geoinformation*, v.14, pp. 112-128, 2012.
- [2] K. Laakso, B. Rivard, J.M. Peter, H.P. White, M. Maloley, J. Harris, and D. Rogge, "Application of airborne, laboratory, and field hyperspectral methods to mineral exploration in the Canadian arctic: Recognition and characterization of volcanogenic massive sulfide-associated hydrothermal alteration in the Izok Lake Deposit area, Nunnavut, Canada", *Economic Geology*, v. 110, pp. 925-941, 2015.
- [3] RIKOLA Ltd., (2016) <http://www.rikola.fi/products/hyperspectral-camera/>
- [4] Cubert GmbH, (2016) <http://cubert-gmbh.de/uhd-185-firefly/>
- [5] H. Aasen, J. Bendig, A. Bolten, S. Bennertz, M. Willkomm, and G. Bareth, "Introduction and preliminary results of a calibration for full-frame hyperspectral cameras to monitor agricultural crops with UAVs", *The International Archives of the Photogrammetry, Remote Sensing and Spatial Information Sciences*, Volume XL-7, 2014 ISPRS Technical Commission VII Symposium, 29 September – 2 October 2014, Istanbul, Turkey.
- [6] E. Honkavaara, J. Kaivosoja, J. Mäkynen, I. Pellikka, L. Pesonen, H. Saari, H. Salo, T. Hakala, L. Markkelin, and T. Rosnell, "Hyperspectral reflectance signatures and point clouds for precision agriculture by light weight UAV imaging system", *ISPRS Annals of the Photogrammetry, Remote Sensing and Spatial Information Sciences*, Volume I-7, 2012 XXII ISPRS Congress, 25 August – 01 September 2012, Melbourne, Australia.
- [7] V. Kopacková, "Using multiple spectral feature analysis for quantitative pH mapping in a mining environment", *International Journal of Applied Earth Observation and Geoinformation*, v. 28, pp. 28-42, 2014.
- [8] Aibotix (2016), <https://www.aibotix.com/de/aibot-x6.html>
- [9] senseFly (2016), <https://www.sensefly.com/drones/ebee.html>
- [10] J.A.J. Berni, P.J. Zarco-Tejada, L. Suárez, V. González-Dugo, and E. Fereres, "Remote sensing of vegetation from UAV platforms using lightweight multispectral and thermal imaging sensors", *Int. Archives of Photogrammetry, Remote Sensing and Spatial Information Sciences*, Hannover, Germany, 38 (1-4-7/W5), 2009.
- [11] M. Vakalopoulou and K. Karantzas, "Automatic descriptor-based co-registration of frame hyperspectral data", *Remote Sensing*, v. 6, pp. 3409-3426, 2014.
- [12] D.G. Lowe, "Object Recognition from Local Scale-Invariant Features", *Proceedings of the International Conference on Computer Vision (ICCV)*, Volume 2, pp. 1150-1157, 1999.
- [13] R. Richter, T. Kellenberger, and H. Kaufmann, "Comparison of topographic correction methods", *Remote Sensing*, v.1, pp. 184-196, 2009.
- [14] H. Aasen, A. Burkart, A. Bolten, and G. Bareth, "Generating 3D hyperspectral information with lightweight UAV snapshot cameras for vegetation monitoring: From camera calibration to quality assurance", *ISPRS Journal of Photogrammetry and Remote Sensing*, v. 108, pp. 245-259, 2015.